ADVANCED FUNCTIONAL MATERIALS
www.afm-journal.de

Materials Views
www.MaterialsViews.com

"Brick-and-Mortar" Self-Assembly Approach to Graphitic Mesoporous Carbon Nanocomposites

*Pasquale F. Fulvio, Richard T. Mayes, Xiqing Wang, Shannon M. Mahurin, John C. Bauer, Volker Presser, John McDonough, Yury Gogotsi, and Sheng Dai**

Mesoporous carbon materials do not have sufficient ordering at the atomic scale to exhibit good electronic conductivity. To date, mesoporous carbons having uniform mesopores and high surface areas have been prepared from partially-graphitizable precursors in the presence of templates. High temperature thermal treatments above 2000 °C, which are usually required to increase conductivity, result in a partial or total collapse of the mesoporous structures and reduced surface areas induced by growth of graphitic domains, limiting their applications in electric double layer capacitors and lithium-ion batteries. In this work, we successfully implemented a "brick-and-mortar" approach to obtain ordered graphitic mesoporous carbon nanocomposites with tunable mesopore sizes below 850 °C without using graphitization catalysts or high temperature thermal treatments. Phenolic resin-based mesoporous carbons act as mortar to highly conductive carbon blacks and carbon onions (bricks). The capacitance and resistivity of final materials can be tailored by changing the mortar to brick ratios.

1. Introduction

Mesoporous materials with crystalline pore walls have attracted large interest for applications in catalysis[1] and energy storage/conversion.[2] Crystalline mesoporous metals and metal oxides have been prepared by various approaches, including the self-assembly of non-ionic triblock copolymers and crystalline oxide clusters,[3] in situ crystallization of oxides from amorphous mesoporous glasses,[4] confined hydrothermal synthesis,[5] controlled crystallization in the presence of chemically and thermally stable hard-templates,[6] or co-condensation of metal alkoxide and crystalline nanoparticles with triblock copolymers ("brick-and-mortar" approach).[1b] Porous carbon materials are widely used in battery and supercapacitor electrodes due to their high conductivity. Mesoporous carbons with atomic periodicity on the pore walls, in particular graphitic structures, allow precise pore size control in the mesopore range and have been prepared by soft[7] and hard-template methods[8] when using partially graphitizable carbon precursors. In all cases, high temperature thermal treatments resulted in a collapse of the mesoporous architecture without significant graphitization.

The hard-template method includes disadvantageous additional steps for the preparation of the templates and the need for hazardous chemicals, such as hydrofluoric acid and sodium hydroxide, to etch the most widely used silica templates. Due to this, the soft-template synthesis of ordered mesoporous carbons (OMCs) using phenolic resins as carbon sources and triblock copolymers as templates is a more economical, faster, and environmentally friendly route to obtain materials with large mesopores and high surface areas. The drawback of the latter is the limitation of available carbon sources that will permit the successful self-assembly of the polymeric framework with the triblock copolymers. The starting precursors are usually limited to partially graphitizable phenol,[7b] phloroglucinol,[7a] resorcinol,[9] with formaldehyde or glyoxal[10] as thermoset resins.

Conductivity of carbon materials heavily depends on the degree of graphitization and electron percolation.[11] Carbon materials that are used for applications such as supercapacitor electrodes include activated carbon, carbide derived carbon, templated carbon,[12] graphene, carbon nanotubes,[11,13] and carbon onions.[14] The latter three exhibit excellent conductivity resulting in their use as electrode materials or conductive fillers. Highly conductive materials like carbon black are usually used in commercial supercapacitors as additives to high-surface area carbons to improve the resulting conductivity of supercapacitors. Recently, it was shown by Pech et al.[15] that binder free onion-like carbon micro-supercapacitors for high-power handling and fast charge-discharge rates, can be obtained via electrophoretic deposition. Depending on the application requirements, control over the porosity of high surface area carbons is essential for optimization of the properties; the pore size distribution in the micropore (<2 nm) and mesopore (2–50 nm)

Dr. P. F. Fulvio, Dr. R. T. Mayes, Dr. X. Wang, Dr. S. M. Mahurin, Dr. J. C. Bauer, Dr. S. Dai
Chemical Sciences Division
Oak Ridge National Laboratory
Oak Ridge, Tennessee 37831, USA
E-mail: dais@ornl.gov
Dr. V. Presser, Mr. J. McDonough, Dr. Y. Gogotsi
Department of Materials Science and Engineering
A.J. Drexel Nanotechnology Institute
Drexel University
Philadelphia, Pennsylvania 19104, USA
Dr. S. Dai
Department of Chemistry
University of Tennessee
Knoxville, TN 37996, USA

DOI: 10.1002/adfm.201002641

range plays a particularly important role.[11,16] Hence, the development of simple yet reproducible and controllable ways to prepare materials exhibiting stable graphitic mesoporous frameworks, especially using the high yield soft-template method, is of particular importance for optimized energy storage devices.

Recently, soft-templated OMCs containing ceramic,[17] metallic[18] and oxide nanoparticles[19] were reported. In the latter case, the chemical composition of the nanoparticles allows their incorporation (20–30 wt%) to the frameworks of the final materials in significant amounts.[19b] The ability of poly(ethylene oxide) – poly(propylene oxide) – poly(ethylene oxide) triblock copolymers to strongly and simultaneously interact with the resorcinol–formaldehyde oligomers and silica/alumina particles yielded homogeneous carbon–oxide nanocomposites. Because strong interactions are necessary, nanoparticles without any surface functional groups segregate during self-assembly synthesis. Consequently, pure carbon nanocomposite materials with homogeneously dispersed graphitic carbon nanostructures and mesoporous carbon nanoparticle assemblies have not been reported yet. Herein, we demonstrate, however, that by using the brick-and-mortar approach,[1b] it is possible to incorporate graphitic carbon nanostructures, i.e., carbon black (CB) and carbon onions (CO) in the framework of OMCs and to systematically replace the phenolic resin precursors by more than 50 wt% of these particles, making it possible to obtain highly conductive mesoporous materials.

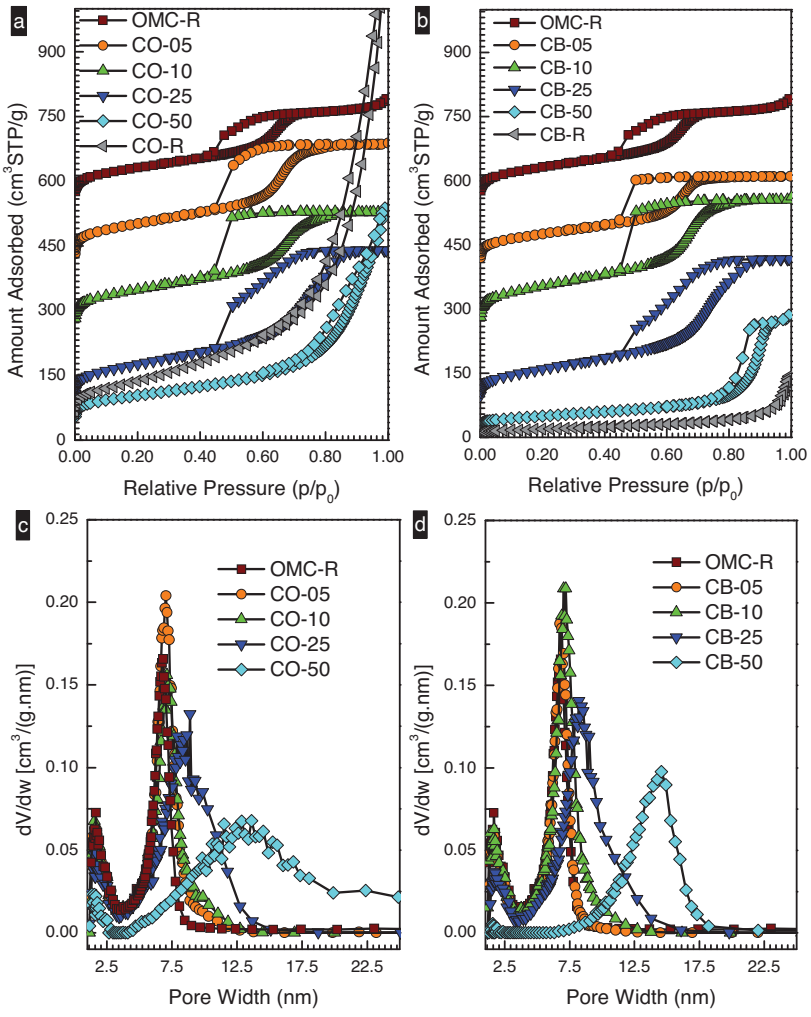

Figure 1. Nitrogen adsorption isotherms at –196 °C for a) CO-*x* and b) CB-*x* and c, d) their corresponding pore size distributions calculated according to the improved KJS method[21a] using statistical film thickness for nonporous carbon reference material.[21b] Adsorption isotherms of CO-10, CO-05 and OMC-R in (a) and of CB-10, CB-05 and OMC-R in (b) were vertically offset by increments of 150 cm^3 STP g^{-1}.

2. Results and Discussion

Nitrogen adsorption isotherms at –196 °C for CO and CB composites (**Figure 1**a and 1b) are characteristic of materials with large mesopores (type IV).[20] In both series, hysteresis loops typical for large mesopores (H-1) are seen for samples containing up to 25 wt% of CO and up to 50 wt% CB in the initial syntheses gels. From the calculated pore size distribution, PSD,[21] (Figure 1c and 1d) we clearly see that with increased CO or CB contents, the PSD changes from a narrow distribution centered at 7 nm to larger and broader pore size distributions. Compared to CO with the same concentration, CB additions to OMC yield more narrow PSDs while the average pore size is comparable up to 50 wt% particle additive (**Table 1**). Also the total pore volumes (single point pore volume) increase proportionally to the CO and CB contents, whereas the highest surface areas were obtained for the smallest loadings of COs and CBs, 5 and 10 wt%. The calculated adsorption parameters are summarized in Table 1. Samples with a high content of carbon onions (CO-50 and CO-75) show an adsorption isotherm similar to the as-received CO material. This indicates that the porosity is governed by agglomerated carbon onions and a resulting loss of the textural templated cylindrical pores. This is corroborated by the electron microphotographs (**Figure 2**) and can, to a lesser degree, also be seen for high concentrations of carbon black. The large pore volume of CO-R is the result of the voids formed by the aggregates of onions that are very small in size, approximately 6 nm, with the textural mesopores being larger than 12 nm in diameter. A control sample was prepared by polymerization of resorcinol with formaldehyde and CB, without the triblock-copolymer, and resulted in a nonporous carbon material (not shown). The pore size enlargement with increased contents of CO and CB in the synthesis gel can be explained by the inability of the PEO chains of the triblock copolymer to interpenetrate the carbon particles, as in the pure phenolic resin. Particles with radii of gyration similar or larger than that of F127 micelles will change the conformation of the block chains, segregating larger particles in a central core and, thus, increasing the effective micelle size.[22]

Table 1. Adsorption parameters calculated from N_2 adsorption at –196 °C isotherms.

Sample	Additive Content [wt%][a)]	V_{SP} [cm^3 g^{-1}][b)]	V_{mi} [cm^3 g^{-1}][c)]	S_{mi} [m^2 g^{-1}][d)]	S_{BET} [m^2 g^{-1}][e)]	w_{KJS} [nm][f)]
CB-R	100	0.16	0.00	0.00	67	30.8
CO-R	100	1.59	0.00	0.00	484	15.1
OMC-R	0	0.52	0.17	252	629	6.8
CO-05	5	0.60	0.19	295	700	7.0
CO-10	10	0.58	0.18	285	688	7.1
CO-25	25	0.68	0.13	324	613	8.9
CO-50	50	0.78	0.05	243	363	13.6
CO-75	75	1.14	0.02	360	402	13.7
CB-05	5	0.48	0.17	234	608	6.7
CB-10	10	0.62	0.18	312	696	7.0
CB-25	25	0.64	0.12	300	556	8.2
CB-50	50	0.43	0.02	121	175	14.6
CB-75	75	0.15	0.01	50	66	29.3
CB-50R	50	0.12	0.03	37	103	30.3

[a)]Additive content in the starting synthesis gels prior to thermal treatments; [b)]Single point pore volume from adsorption isotherms at p/p_0 ~0.98; [c,d)]Micropore volume and micropore surface area calculated in the α_S-plot range of 0.75–1.00 of standard adsorption, α_S;[29] [e)]Specific surface area calculated using the BET equation in the relative pressure range of 0.05–0.20; [f)]Pore width calculated according to the improved KJS method[21a] and statistical film thickness for nonporous carbon reference.[21b]

The mesopore structures of CO-*x* and CB-*x* materials were investigated by STEM (Figure 2). The images show that CO and CB particles are well dispersed in the highly ordered mesoporous carbon matrices. All CO-*x* and CB-*x* samples up to 25 wt% exhibit 2-dimensional (2D) hexagonal arrangement of cylindrical mesopores, P6mm symmetry. The CO-50 sample (Figure S 1 in Supporting Information) is composed of CO walls interconnected by carbon from the resorcinol-formaldehyde resin. Differences were found when large CB particles were present in the gels where a thin film of mesoporous carbon acts as the mortar for the CB bricks. The powder X-ray diffraction (XRD) for the reference samples and selected nanocomposites with high loadings of CB and CO particles are shown in Figure S2 in Supporting Information. The patterns for the CB-R and CO-R were assigned to that of graphitic carbons (JCPDS 4–7-2081 and 1–646, respectively), with calculated d_{002}-spacings of 0.349 nm and 0.341 nm, respectively. No diffraction peaks could be identified on the XRD pattern for OMC-R sample, whereas low intensity and broad reflections from the added graphitic nanostrutures (CB and CO) were identified in case of CB-25 and CO-25, despite of the intense background from the amorphous mesoporous carbon framework. For the latter two composites, the d_{002}-spacings were estimated as 0.347 nm and 0.338 nm, respectively; all materials exhibit larger d_{002}-spacings than that for natural graphite of 0.335 nm.[8a] Broader diffraction peaks, as well peak shifts to wider 2θ angles afforded larger calculated *d*-spacings, resulting from lattice defects, presence of amorphous carbons and small crystallite sizes. Further evidence for the existence of graphitic domains in these materials was provided by Raman spectroscopy. While Raman spectra of CO-*x* samples are indistinguishable, see (Figure 2g), the spectrum for CB-50 sample largely resembles that of pure CB powder (not shown). CB exhibits narrower D (~1320 cm^{-1}) and G (~1590 cm^{-1}) bands, a relatively intense 2D band (~2650 cm^{-1}) and the additional D+G band at approximately 2890–2900 cm^{-1}.[23]

Such structural changes are also reflected in the electrochemical behavior of these nanocomposites. For instance, the capacitance changes significantly as a function of CO and CB contents as seen in **Figure 3**a and b. Increasing the CO content in the pore walls of the nanocomposites resulted in retention of the large gravimetric capacitance for CO-25 at sweep rates as high as 200 mV s^{-1}, in contrast to CO-5 (Figure 3b) and OMC-R (not shown). A constant capacitance over a large scan rate range is one of the advantages of carbon onions and is displayed for higher CO concentrations (>25 wt%).[15] The final nanocomposites having concentric graphitic carbon structures exhibit superior double layer capacitance performance when compared to pure mesoporous materials with pore walls having amorphous or turbostratic carbon. When comparing the Nyquist plots for materials with similar contents of CO and CB, see Figure 3c, the slope of the plot for CO is steeper than for CB, indicating a larger charge transfer resistance, i.e., a larger diffusion limitation, in the sample with CB. Also, higher loadings of the CO and CB lowered the equivalent series resistance of these composites, shown by the semi-circles in the Nyquist plots (Figure 3d and e, respectively) and calculated values[24] (Figure 3f). Furthermore, CO-*x* materials exhibited lower resistivity than the CB-*x* nanocomposites. This shows that even at such high loadings, the mesoporous carbon (mortar) did not interrupt the CO particle network (bricks) permitting electron percolation, in comparison to the much larger and more segregated CB particles. Also the series resistance values for CO-25 and CB-25 were similar to those of the carbon bricks used, CO-R and CB-R, respectively. In addition, CO-*x* composites clearly show semi-circle shapes at high frequencies in the Nyquist plots, in contrast to those previously reported for the pure carbon onions.[14b] Phase angle versus frequency curves

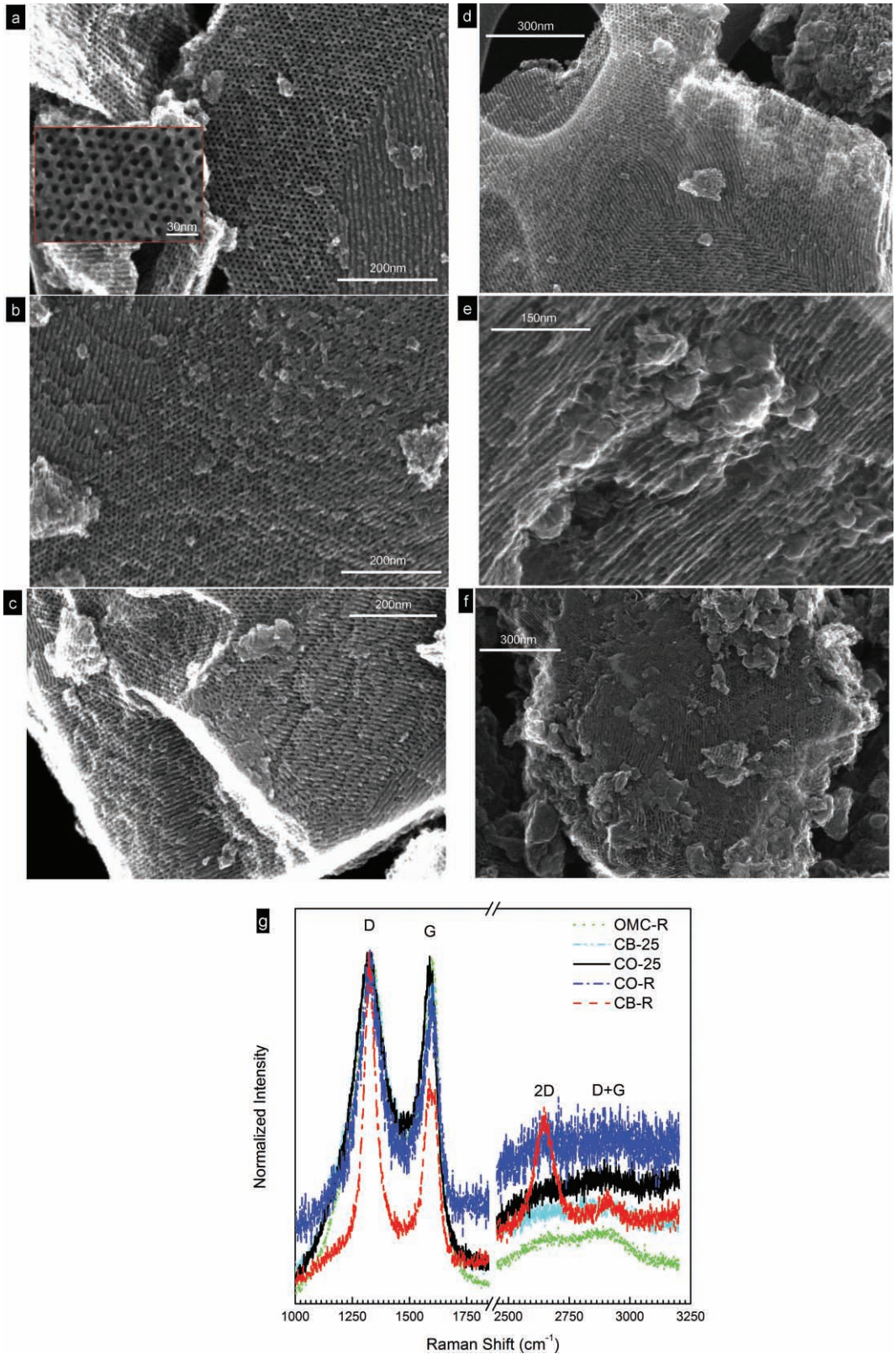

Figure 2. Representative SEM images for carbon onion nanocomposites CO-*x*. a) $x = 5$, b) 10 and c) 25 wt%. Representative SEM for d) CB-05, e) CB-10 and f) CB-25. g) Normalized Raman spectra for selected reference materials and CO-25 and CB-25 nanocomposites, showing the characteristic D and G bands for carbon materials, with additional intense 2D and D + G bands for the starting carbon black sample.

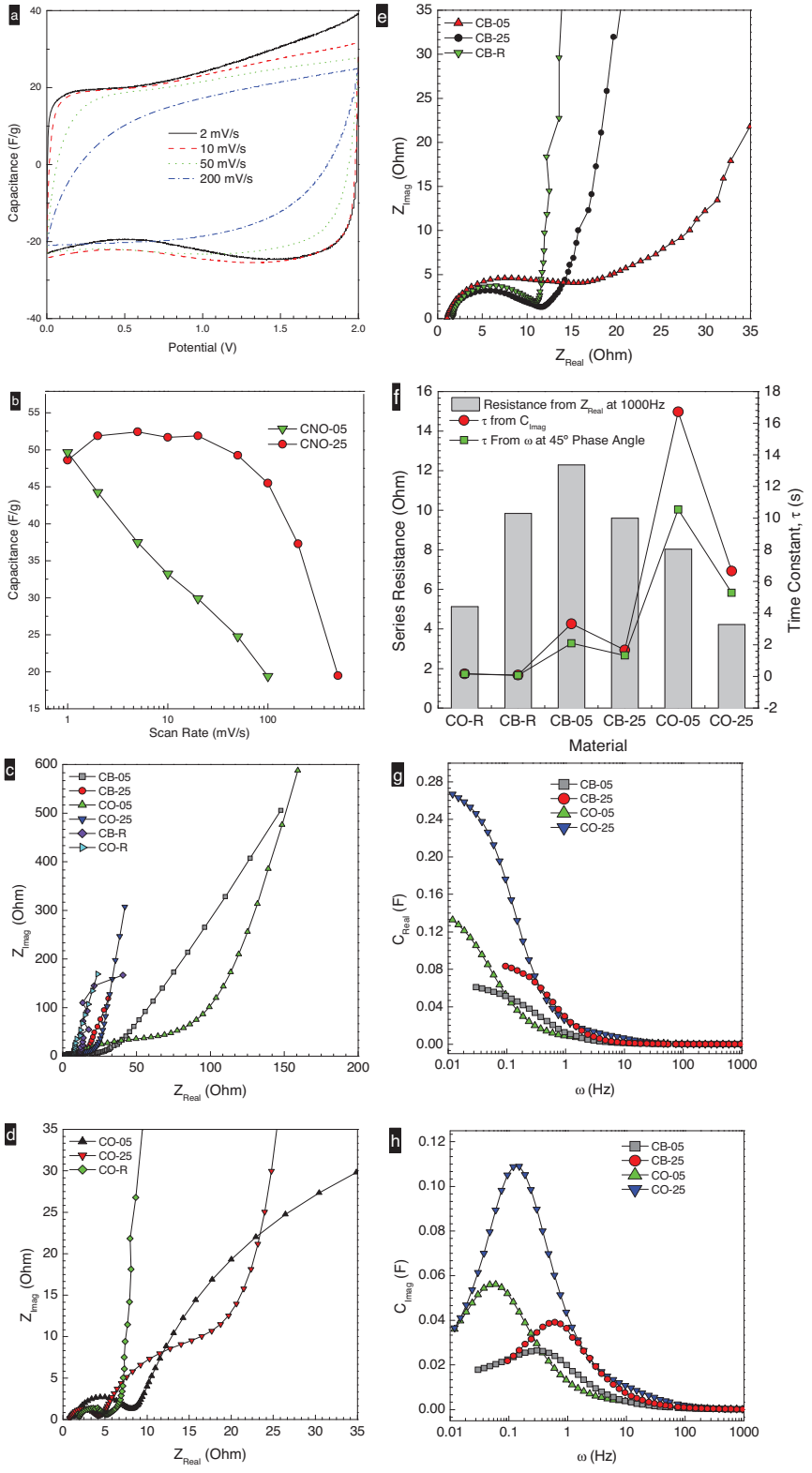

Figure 3. a) Representative cyclic voltamograms for CO-25 nanocomposite and b) capacitance results as a function of the sweep rates for CO-5 in comparison to CO-25. c) Nyquist plots. d and e) Magnification of semi-circles in the same Nyquist curves, for selected CO-*x* and CB-*x* nanocomposites compared to CO-R (a) and CB-R (b) materials. f) Lower resistivity is found for higher onion and carbon black contents, g) CO composite electrodes have a better capacitive behavior than the real capacitance, C_{Real}, represents the actual capacitance of the cell. h) From the maxima in the imaginary component of the capacitance, C_{Imag}, vs frequency, ω, plots, the calculated time constants, τ, for CO-R, CB-R, onion-based composites are higher than mesoporous carbon black composites (f); a similar correlation was obtained for the time constants calculated using frequencies at –45° phase angles.

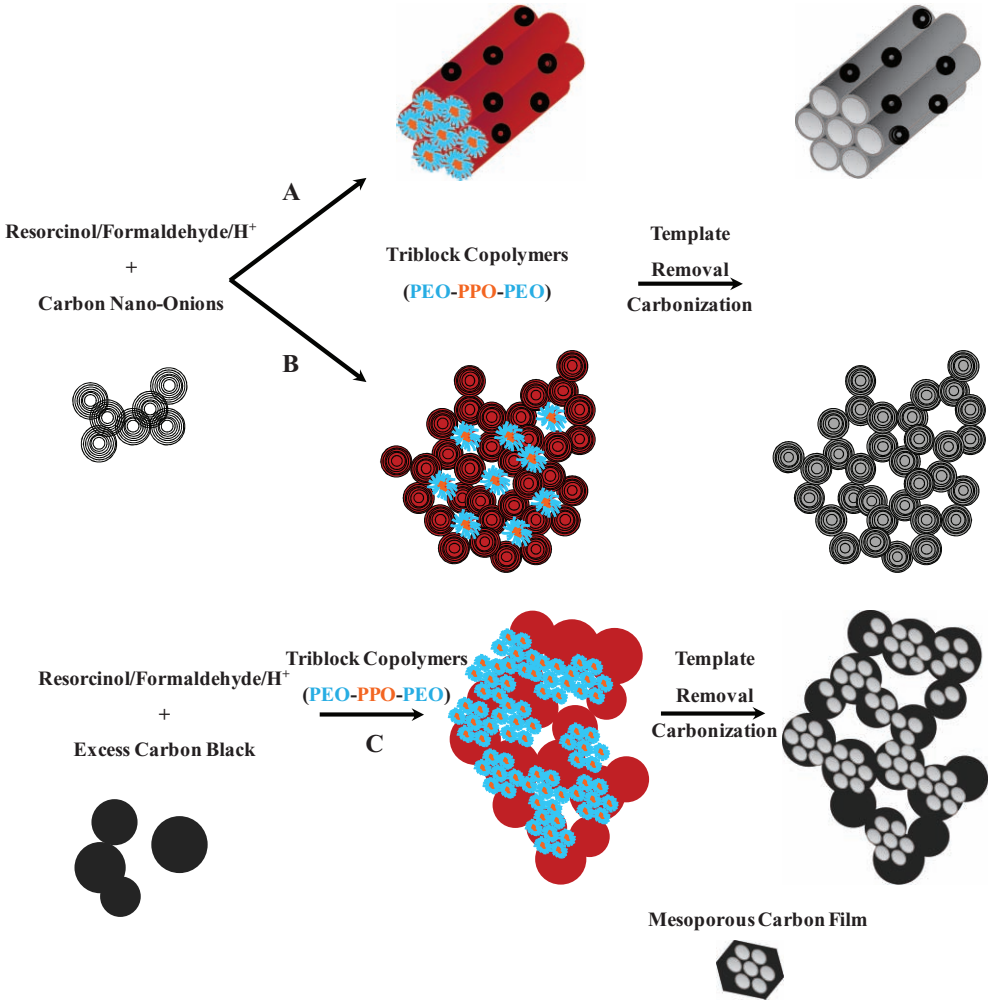

Figure 4. Proposed self-assembly mechanism of CO-*x* and CB-*x* nanocomposites using excess resorcinol-formaldehyde (A). The CO and CB nanoparticles are dispersed throughout the OMC matrix. When in excess, CO (B) and CB (C) particles assemble differently with resorcinol-formaldehyde resin. For the small CO particles, a non-porous thin carbon film acts as a mortar and the mesopores are formed by the irregular assembly of CO. For the much larger and less regular CB particles, a thin mesoporous carbon film acts as the mortar for the CB bricks. In the latter case, much larger pores are formed between aggregates of mesoporous carbon-coated CB particles.

show capacitive behavior for these samples at low and high frequencies (not shown), whereas CB materials exhibit resistive behavior at intermediate frequencies where CO materials maintain their capacitive properties without significant phase shifts based on CO contents. Electrodes with CO as an additive have a better capacitive behavior, as the real capacitance, C_{Real}, represents the actual capacitance of the cell, (Figure 3g). Also, the frequency response of the CO electrodes is higher than for the CB electrodes, indicating better rate capabilities. From the imaginary part of the capacitance, C_{Imag} in Figure 3h), the time constants (τ) are calculated, see (Figure 3f), illustrating a maximum value at a given frequency.[24] These values correlate well with the capacitance values calculated from the frequencies (ω) at –45° in the phase angle plots. Furthermore, all nanocomposites exhibit at least 10 times the capacitance of CO-R and CB-R samples (not shown), and consequently, higher time constants.

The general formation mechanism of soft-templated OMCs is the in situ polymerization of resorcinol, phloroglucinol with formaldehyde, or glyoxal in the presence of triblock copolymer surfactants in acidic conditions via enhanced hydrogen bonding and charge interactions.[7a,9] OMCs are finally obtained after phase separation of an organic polymer nanocomposite, followed by annealing and thermal treatments of films in non-oxidizing atmosphere. The surfaces of the carbon nano-onions (CO) and carbon black (CB) do not exhibit groups to allow for the hydrogen bonding interaction between these and triblock copolymers. Our results indicate that precursors such as resorcinol can be physically adsorbed on their surfaces, thus providing the interaction with the block copolymer templates according to the mechanism in (**Figure 4**), with micro phase polymerization and separation occurring without significant solid–gel phase segregation. The final gels are then converted into highly ordered mesoporous carbons binding the small and large agglomerates of COs or CBs following the proposed brick-and-mortar approach.[1b] This mesoporous carbon "mortar" acts as a binder for the carbon onions and as a mesoporous carbon

film, coating and binding the larger CB particles; in both cases forming stable porous frameworks. The final composites exhibit thermally stable mesopores and much higher electrical conductivity than pure phenolic resin-based carbons and without the need for graphitization above 2000 °C, thus preserving the porosity. Furthermore, only carbons templated with large silica colloids exhibited mesopores larger than 10 nm diameter.[8e] In general, tailoring the pore diameters of mesoporous carbons represents a significant challenge. Recently, it has been demonstrated that the ordered mesopores of soft-templated carbon materials can also be increased by mixing different triblock copolymers.[25] Final carbons however, still exhibited ordered pores smaller than 8 nm.[25] The present brick-and-mortar approach for the synthesis of mesoporous carbons resulted in materials with mesopores larger than previously reported for templated carbons. The brick-and-mortar approach combined with the soft-template synthesis does not require mixtures of surfactants and, as previously mentioned, requires less preparative steps while avoiding hazardous chemicals used in the hard-templating method.[8g] Thus, the present methodology is not only more economically viable compared to all previous methods, but also more environmentally friendly than hard-templated carbons.

3. Conclusions

In summary, these results show it is possible to greatly improve and tailor the electrochemical performance of low-temperature mesoporous carbons that, in general, lack sufficient ordering at the atomic level thereby having moderate electrical conductivity, which limits their applications. The addition of carbon blacks and carbon onions to the synthesis gels of mesoporous carbons also provides a general methodology to tune the pore widths of the final materials, which is difficult to attain for pure resin based carbons. Such nanocomposites may further be prepared as powders, monoliths, and as films. Furthermore, the ability to prepare soft-templated carbons with mesopores in the range of 10–20 nm without organic additives or using mixtures of surfactants represents a major economical advantage of the present method. Carbon materials with such large pores are extremely attractive for the design of membranes,[26] catalyst supports,[27] enzyme immobilization[28] and assembly of future electrode materials for energy storage applications[12–16,24] ranging from portable electronic devices to hybrid vehicles.

4. Experimental Section

Synthesis: Carbon onions were obtained by vacuum annealing of detonation nanodiamonds (DND) at 1500 °C yielding 4–6 nm large carbon onions.[14b] Mesoporous carbon samples were prepared by the self-assembly of resorcinol (Sigma–Aldrich, 99%) and formaldehyde (Sigma–Aldrich, 37 wt%) in the presence of triblock copolymer Pluronic F127 (EO_{106}-PO_{70}-EO_{106}, BASF) purchased from Sigma–Aldrich, according to previously reported recipe.[9] In a typical synthesis, approximately 1.1 g of resorcinol and 1.1 g of Pluronic F127 were dissolved in 4.5 mL of ethanol, 3.4 mL of water and 1.1 mL of concentrated HCl (37 wt%). To this, 1.3 mL of formaldehyde solution (37 wt%) was added and the system stirred until phase separation was observed. The carbon black (Sigma Aldrich, acetylene, <200 nm) and carbon onion composites were prepared by substituting the resorcinol by weight%, (5–95 wt%) and the amount of formaldehyde adjusted proportionally to the amount of resorcinol used. After stirring for an additional 30 min, the suspensions were centrifuged at 9500 rpm for 5 min and the aqueous phases discarded. The isolated polymer-rich phases were quickly re-dispersed using minimal amounts of ethanol with strong stirring followed by casting on Petri dishes. Thin films were cured at room temperature for 6 hours (and reference resorcinol/formaldehyde-F127 film overnight) and at 150 °C for 24 h. The phenolic resin-triblock copolymer nanocomposites were finally carbonized at 400 °C for 2 h (1 °C min^{-1} heating rate) and 850 °C for 2 h in flowing nitrogen and using 2 °C min^{-1} as heating rate. Ordered mesoporous carbon was labeled OMC-R and composites were labeled as CB-*x* and CO-*x*, respectively, where *x* stands for the initial weight% of CB or CO with respect to resorcinol in the synthesis gels (5, 10, 25, 50 and 75 wt%). A sample containing 50 wt% of CB to resorcinol was prepared in a similar way but without F127 template and after carbonization, the latter was labeled CB-50R. Pure carbon blacks and carbon onions were labeled as CB-R and CO-R, respectively.

Characterization: Nitrogen adsorption isotherms were measured at –196 °C using TriStar 3000 volumetric adsorption analyzer manufactured by Micromeritics Instrument Corp. (Norcross, GA). Before adsorption measurements the, finely ground carbon powders were degassed in flowing nitrogen from one to two hours at 200 °C. The specific surface area of the samples was calculated using the Brunauer-Emmett-Teller (BET) method within the relative pressure range of 0.05 to 0.20.[20] Pore size distributions were calculated using the BJH algorithm for cylindrical pores according to the KJS method calibrated for pores up to 10 nm.[21] For TEM characterization, carbon powders were dispersed in ethanol using an ultrasonic bath. The final suspensions were transferred to lacy carbon coated 200-mesh copper TEM grids and dried in ambient air prior to electron microscopy analysis. Specimens were then characterized using a Hitachi HD-2000 operating in STEM mode using a secondary electron (SE) and/or bright-field STEM detector operating at 200 kV. The wide angle XRD patterns were recorded on a PANanalytical. Inc. X'Pert Pro (MPD) Multi Purpose Diffractometer with X'Celerator detector and Cu Kα radiation (0.1540 nm), using an operating voltage of 40 kV and 40 mA, and 0.01° step size ($15.00° < 2\theta < 55.00°$). Microscope glass slides were used as sample supports for small angle measurements and for wide angle measurements of OMC, CB-*x* and CO-*x* nanocomposites, whereas Al holders (PANanalytical PW1172, 15 mm × 20 mm × 1.8 mm) were used for wide angle measurements of the CB-R and CO-R reference materials. The samples were manually ground prior to the XRD analysis and all measurements were performed at room temperature. Raman spectra were collected using a Renishaw system 1000 Raman spectrometer equipped with an integral microscope (Leica DMLMS/N). Excitation was provided by a 25 mW He–Ne laser (Renishaw) and the 632.8 nm excitation beam was focused onto the sample with a 50 × objective; the laser power at the sample was approximately 0.2–0.5 mW for carbon onions and carbon black and 2 mW for nanocomposites. An edge filter removed the Rayleigh scattered light, while a holographic grating (1800 grooves mm^{-1}) permitted a spectral resolution of ~1 cm^{-1}. A silicon wafer with a Raman band at 520 cm^{-1} was used to calibrate the spectrometer and the accuracy of the spectral measurements was estimated to be better than 1 cm^{-1}. For the capacitive energy storage measurements, a slurry of the carbon and polyvinylidene fluoride (PVDF; 15 wt%) in N-methylpyrrolidone (NMP) was cast onto aluminum foil and dried under a heat lamp. Electrodes (13 mm diameter) were then cut out and subsequently dried at 120 °C under vacuum. The dry electrodes were then transferred to an inert atmosphere (Argon) glove box for construction of coin-type cells. The electrolyte was triethylmethylammonium tetrafluoroborate in acetonitrile (1.8 mol L^{-1}). Impedance spectroscopy measurements were collected using the aforementioned coin cells on a Gamry Reference 600 potentiostat in the frequency range of 0.1–10^6 Hz. Cyclic voltammetry (CV) was performed on the Gamry G300 potentiostat with a potential range of 0.0–2.0 V. The gravimetric capacitance was calculated from the CV curve following the formula:

$$C_g = \frac{\left(\frac{\Delta I}{2}\right)}{m\nu} \quad (1)$$

where ΔI is the current difference at 1 V, m is the mass of the active material, and v is the scan rate.

Supporting Information

Supporting Information is available from the Wiley Online Library or from the author.

Acknowledgements

P.F.F., S.M.M., V.P., J.M., Y.G. and S.D. were supported as part of the Fluid Interface Reactions, Structures and Transport (FIRST) Center, an Energy Frontier Research Center funded by the U.S. Department of Energy, Office of Science, Office of Basic Energy Sciences under contract DE-AC05-OR22725 with Oak Ridge National Laboratory, managed and operated by UT-Battelle, LLC. X.W. was supported by the Division of Chemical Sciences, Geosciences, and Biosciences, Office of Basic Energy Sciences, U.S. Department of Energy. R.T.M. was supported by the U. S. DOE Office of Energy Efficiency and Renewable Energy (EERE). V.P. gratefully acknowledges financial support by the Alexander von Humboldt Foundation.

Received: December 16, 2010
Revised: February 22, 2011
Published online: April 20, 2011

[1] a) Z. T. Zhang, Y. Han, L. Zhu, R. W. Wang, Y. Yu, S. L. Qiu, D. Y. Zhao, F. S. Xiao, *Angew. Chem. Int. Ed.* **2001**, *40*, 1258; b) J. M. Szeifert, D. Fattakhova-Rohlfing, D. Georgiadou, V. Kalousek, J. Rathousky, D. Kuang, S. Wenger, S. M. Zakeeruddin, M. Gratzel, T. Bein, *Chem. Mater.* **2009**, *21*, 1260.

[2] a) H. S. Zhou, D. L. Li, M. Hibino, I. Honma, *Angew. Chem. Int. Ed.* **2005**, *44*, 797; b) S. C. Warren, L. C. Messina, L. S. Slaughter, M. Kamperman, Q. Zhou, S. M. Gruner, F. J. DiSalvo, U. Wiesner, *Science* **2008**, *320*, 1748.

[3] D. Grosso, C. Boissiere, B. Smarsly, T. Brezesinski, N. Pinna, P. A. Albouy, H. Amenitsch, M. Antonietti, C. Sanchez, *Nat. Mater.* **2004**, *3*, 787.

[4] D. L. Li, H. S. Zhou, I. Honma, *Nat. Mater.* **2004**, *3*, 65.

[5] W. Fan, M. A. Snyder, S. Kumar, P.-S. Lee, W. C. Yoo, A. V. McCormick, R. Lee Penn, A. Stein, M. Tsapatsis, *Nat. Mater.* **2008**, *7*, 984.

[6] J. Lee, M. Christopher Orilall, S. C. Warren, M. Kamperman, F. J. DiSalvo, U. Wiesner, *Nat. Mater.* **2008**, *7*, 222.

[7] a) C. Liang, S. Dai, *J. of the Am. Chem. Soc.* **2006**, *128*, 5316; b) Y. Meng, D. Gu, F. Zhang, Y. Shi, L. Cheng, D. Feng, Z. Wu, Z. Chen, Y. Wan, A. Stein, D. Zhao, *Chem. Mater.* **2006**, *18*, 4447; c) Y. Meng, D. Gu, F. Zhang, Y. Shi, H. Yang, Z. Li, C. Yu, B. Tu, D. Zhao, *Angew. Chem. Int. Ed.* **2005**, *44*, 7053.

[8] a) K. P. Gierszal, M. Jaroniec, T. W. Kim, J. Kim, R. Ryoo, *New J. Chem.* **2008**, *32*, 981; b) T. W. Kim, I. S. Park, R. Ryoo, *Angew. Chem. Int. Ed.* **2003**, *42*, 4375; c) Z. J. Li, M. Jaroniec, Y. J. Lee, L. R. Radovic, *Chem. Commun.* **2002**, 1346; d) S. B. Yoon, G. S. Chai, S. K. Kang, J. S. Yu, K. P. Gierszal, M. Jaroniec, *J. Am. Chem. Soc.* **2005**, *127*, 4188; e) K. P. Gierszal, M. Jaroniec, *J. Am. Chem. Soc.* **2006**, *128*, 10026; f) F. Schuth, *Angew. Chem. Int. Ed.* **2003**, *42*, 3604; g) M. Tiemann, *Chem. Mater.* **2008**, *20*, 961.

[9] X. Q. Wang, C. D. Liang, S. Dai, *Langmuir* **2008**, *24*, 7500.

[10] R. T. Mayes, C. Tsouris, J. O. Kiggans, S. M. Mahurin, D. W. DePaoli, S. Dai, *J. Mater. Chem.* **2010**, *20*, 8674.

[11] A. G. Pandolfo, A. F. Hollenkamp, *J. Power Sources* **2006**, *157*, 11.

[12] Y. Korenblit, M. Rose, E. Kockrick, L. Borchardt, A. Kvit, S. Kaskel, G. Yushin, *ACS Nano* **2010**, *4*, 1337.

[13] a) E. Frackowiak, F. Beguin, *Carbon* **2001**, *39*, 937; b) P. Simon, Y. Gogotsi, *Nat. Mater.* **2008**, *7*, 845.

[14] a) C. Portet, J. Chmiola, Y. Gogotsi, S. Park, K. Lian, *Electrochim. Acta* **2008**, *53*, 7675; b) C. Portet, G. Yushin, Y. Gogotsi, *Carbon* **2007**, *45*, 2511.

[15] D. Pech, M. Brunet, H. Durou, P. Huang, V. Mochalin, Y. Gogotsi, P.-L. Taberna, P. Simon, *Nat. Nano* **2010**, *5*, 651.

[16] P. Simon, Y. Gogotsi, *Philos.Trans. R. Soc., A* **2010**, *368*, 3457.

[17] Q. Zhu, S. H. Zhou, X. Q. Wang, S. Dai, *J. Power Sources* **2009**, *193*, 495.

[18] a) Y. Y. Shao, S. Zhang, R. Kou, X. Q. Wang, C. M. Wang, S. Dai, V. Viswanathan, J. Liu, Y. Wang, Y. H. Lin, *J. Power Sources* **2010**, *195*, 1805; b) J. S. Li, J. Gu, H. J. Li, Y. Liang, Y. X. Hao, X. Y. Sun, L. J. Wang, *Microporous Mesoporous Mater.* **2010**, *128*, 144; c) G. Gupta, D. A. Slanac, P. Kumar, J. D. Wiggins-Camacho, X. Q. Wang, S. Swinnea, K. L. More, S. Dai, K. J. Stevenson, K. P. Johnston, *Chem. Mater.* **2009**, *21*, 4515; d) X. Q. Wang, S. Dai, *Adsorption* **2009**, *15*, 138.

[19] a) M. N. Patel, X. Q. Wang, B. Wilson, D. A. Ferrer, S. Dai, K. J. Stevenson, K. P. Johnston, *J. Mater. Chem.* **2010**, *20*, 390; b) J. Gorka, M. Jaroniec, *J. Phys. Chem. C* **2008**, *112*, 11657; c) M. Jaroniec, J. Gorka, J. Choma, A. Zawislak, *Carbon* **2009**, *47*, 3034.

[20] M. Kruk, M. Jaroniec, *Chem. Mater.* **2001**, *13*, 3169.

[21] a) M. Jaroniec, L. A. Solovyov, *Langmuir* **2006**, *22*, 6757; b) J. Choma, J. Gorka, M. Jaroniec, *Microporous Mesoporous Mater.* **2008**, *112*, 573.

[22] A. Jain, U. Wiesner, *Macromolecules* **2004**, *37*, 5665.

[23] T. Livneh, T. L. Haslett, M. Moskovits, *Phys. Rev. B* **2002**, *66*.

[24] P. L. Taberna, P. Simon, J. F. Fauvarque, *J. Electrochem. Soc.* **2003**, *150*, A292.

[25] Y. Huang, H. Q. Cai, T. Yu, X. L. Sun, B. Tu, D. Y. Zhao, *Chem. Asian J.* **2007**, *2*, 1282.

[26] a) M. Yoshimune, T. Yamamoto, M. Nakaiwa, K. Haraya, *Carbon* **2008**, *46*, 1031; b) X. Q. Wang, Q. Zhu, S. M. Mahurin, C. D. Liang, S. Dai, *Carbon* **2010**, *48*, 557.

[27] a) F. B. Su, J. H. Zeng, X. Y. Bao, Y. S. Yu, J. Y. Lee, X. S. Zhao, *Chem. Mater.* **2005**, *17*, 3960; b) S. H. Joo, S. J. Choi, I. Oh, J. Kwak, Z. Liu, O. Terasaki, R. Ryoo, *Nature* **2001**, *412*, 169.

[28] a) M. Hartmann, *Chem. of Mater.* **2005**, *17*, 4577; b) J. Lee, D. Lee, E. Oh, J. Kim, Y. P. Kim, S. Jin, H. S. Kim, Y. Hwang, J. H. Kwak, J. G. Park, C. H. Shin, T. Hyeon, *Angew. Chem. Int. Ed.* **2005**, *44*, 7427; c) A. Vinu, M. Miyahara, T. Mori, K. Ariga, *J. Porous Mater.* **2006**, *13*, 379.

[29] M. Kruk, M. Jaroniec, K. P. J. Gardkaree, *Colloid Interface Sci.* **1997**, *192*, 250.